Since January 2020 Elsevier has created a COVID-19 resource centre with free information in English and Mandarin on the novel coronavirus COVID-19. The COVID-19 resource centre is hosted on Elsevier Connect, the company's public news and information website.

Journal of Colloid and Interface Science 592 (2021) 342–348

Contents lists available at ScienceDirect

Journal of Colloid and Interface Science

journal homepage: www.elsevier.com/locate/jcis

Regular Article

Carbon dot-polymer nanoporous membrane for recyclable sunlight-sterilized facemasks

Seema Singh [a,1], Nitzan Shauloff [a,1], Chetan Prakash Sharma [b], Ran Shimoni [a], Christopher J. Arnusch [b], Raz Jelinek [a,c,*]

[a] Department of Chemistry, Ben-Gurion University of the Negev, Beer Sheva 8410501, Israel
[b] Department of Desalination and Water Treatment, Zuckerberg Institute for Water Research, The Jacob Blaustein Institutes for Desert Research, Ben-Gurion University of the Negev, Sede-Boqer Campus, Beersheba 84990, Israel
[c] Ilse Katz Institute for Nanotechnology, Ben-Gurion University of the Negev, Beer Sheva 8410501, Israel

GRAPHICAL ABSTRACT

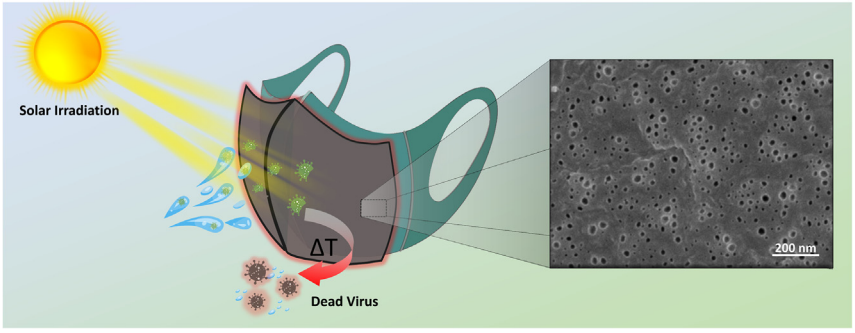

ARTICLE INFO

Article history:
Received 14 January 2021
Revised 6 February 2021
Accepted 11 February 2021
Available online 26 February 2021

Keywords:
Self-sterilized facemasks
Nanoporous membranes
Carbon dots
Photothermal nanoparticles

ABSTRACT

Facemasks are considered the most effective means for preventing infection and spread of viral particles. In particular, the coronavirus (COVID-19) pandemic underscores the urgent need for developing recyclable facemasks due to the considerable environmental damage and health risks imposed by disposable masks and respirators. We demonstrate synthesis of nanoporous membranes comprising carbon dots (C-dots) and poly(vinylidene fluoride) (PVDF), and demonstrate their potential use for recyclable, self-sterilized facemasks. Notably, the composite C-dot-PVDF films exhibit hydrophobic surface which prevents moisture accumulation and a compact nanopore network which allows both breathability as well as effective filtration of particles above 100 nm in diameter. Particularly important, self-sterilization occurs upon short solar irradiation of the membrane, as the embedded C-dots efficiently absorb visible light, concurrently giving rise to elevated temperatures through heat dissipation.

1. Introduction

The COVID-19 pandemic started in December 2019 and rapidly spread globally. The virus is believed to be transmitted by respiratory droplets through sneezing, coughing and talking [1,2]. Those droplets vary in size and the smaller aerosol can float in air for extended time periods [3]. Facial masks combine aerosol filters

* Corresponding author at: Department of Chemistry, Ben-Gurion University of the Negev, Beer Sheva 8410501, Israel.
E-mail address: razj@bgu.ac.il (R. Jelinek).
[1] Seema Singh and Nitzan Shauloff contributed equally.

https://doi.org/10.1016/j.jcis.2021.02.049
0021-9797/

and/or fabrics, designed to block the droplets and associated viral particles from entering the human body thus preventing infection [4,5]. However, fabrication of enormous quantities of facemasks which are, by and large, non-reusable, has resulted in enormous hazardous waste and adverse environmental impact [6]. To address this, chemical disinfectants and incineration are being used for eliminating facemask waste, which in turn induce further environmental harm through, for example, toxic gas release [7]. In an attempt to overcome the hazards associated with non-reusable masks, the World Health Organization (WHO) recommended the use of cloth masks [8]. However, research has shown limited effectiveness of cloth-made facemasks for blocking the spread of infectious diseases [9,10]. In particular, cloth materials offer limited protection against nanometer-scale viral particles which can easily pass through [11,12]. Furthermore, viral particles might adhere to cloth fibers thereby increasing risk of infection [10]. As such, development of reusable, environmentally friendly facemasks which can effectively block viral transmission is considered a major goal.

Sunlight-mediated sterilization of facemasks has gained interest as a promising avenue for recyclability [13,14]. Photothermal materials used in potential facemask applications include graphene coated on surgical masks [13] and silver nanoparticles deposited upon N95 masks [14]. These materials, however, are difficult to fabricate and cumbersome for practical use. Similarly, various antiviral and antibacterial masks have been developed by coating conventional facemask materials with chemical agents [15,16]. However, use of such disinfectants in facial mask is undesirable due to possible physiological toxicity and environmental pollution [16].

In this work, we employed for the first time carbon dots (C-dots) as photothermal agents in nanoporous polymer-based sunlight recyclable viral-blocking matrix. C-dots are a unique class of carbon nanoparticles, synthesized from readily available carbonaceous building blocks, exhibiting remarkable optical properties, biocompatibility, and diverse biological and chemical applications [17–19]. In particular, the excellent photothermal properties of C-dots have been recently employed in solar-enabled water remediation [20], optical-switching [21] and oil-spill cleanup applications [22]. Here, we report construction of a composite nanoporous membrane comprising C-dots and polyvinylidene fluoride (PVDF) via a simple mixed solvent phase separation scheme. PVDF has been extensively used in varied applications due to its stability and resilience, mechanical strength and thermal stability [23]. PVDF membranes have been utilized in water treatment [24], gas separation [25], lithium ion batteries [26], pollutant removal [27] and oil/water separation [28]. The nanoporous C-dot-PVDF membrane displays hydrophobicity, air permeability, effective nanoparticle filtration, and, particularly important, solar-induced sterilization through sunlight absorbance and concomitant heat dissipation afforded by the embedded C-dots. The new C-dot-PVDF membrane constitutes an inexpensive, readily prepared, environmentally friendly, reusable and self-sterilizing platform which may be employed in viral-blocking facemasks and respirators.

2. Materials and methods

2.1. Materials

Citric acid and urea, ACS reagents ≥99.5%, were purchased from Sigma-Aldrich. Dimethyl sulfoxide (DMSO), purity ≥99.98%, was obtained from Glentham Life Sciences. N,N,Dimethylformamide (DMF), AR ≥ 99.5% was purchased from Bio-Lab ltd. Israel. *n*-Octane (purity = 98%), polyvinylidene fluoride (PVDF) and ethanol (ACS reagent 96%) were supplied by Alfa Aesar.

2.2. Synthesis of carbon dots

C-dots were synthesized by hydrothermal heating of citric acid and urea as precursors according to a previously reported method [29]. Citric acid (2 g) and urea (6 g) were added and dissolved in 30 mL of DMSO (DMSO furnishes a lower energy level due to S-doping, thus reducing the optical bandgap and contributing to broad absorbance range in both visible and near IR regions [29]. The transparent solution obtained was then transferred to a Teflon-lined autoclave and heated at 160 °C for 4 h followed by cooling to room temperature. The black-brown C-dot suspension was mixed with excess of ethanol and centrifuged at 10,000 rpm for 15 min. On centrifugation, the precipitate of C-dots was obtained and dried.

2.3. Preparation of C-dot-PVDF membranes

The C-dot-PVDF membrane was synthesized through modification of a mixed solvent phase separation (MSPS) method [30]. PVDF (0.75 g), C-dots (0.0375 g), DMF (2.91 mL) and *n*-Octane (2.1 mL) were mixed and heated to 85 °C for 24 h to get a homogenous casting solution. A thin film of C-dot-PVDF was casted on a preheated glass plate at 85 °C by a doctor blade method [31]. The film was covered with a glass petri dish and left at room temperature for 90 s. This C-dot-PVDF on glass plate was immersed in room-temperature distilled water to detach the membrane from the glass substrate. The membrane was then kept in fresh distilled water for 12 h and subsequently in ethanol for another 12 h to remove solvent traces and unreacted loosely bound moieties. Finally, the membrane was dried in ambient conditions. Similarly, control PVDF membrane was prepared without addition of C-dots.

2.3.1. Escherichia coli viability assay

Single bacterial colonies *Escherichia coli* (*E. coli*) extracted from Luria-Bertani (LB) agar plates were inoculated in 10 mL of LB broth and kept at 37 °C for 12 h in a shaking incubator (220 rpm). The concentration of bacteria in the medium was obtained by measuring the optical density at 600 nm (OD 600). When the OD 600 reached 0.5, 50 μl from the bacterial culture was placed on a the C-dot-PVDF membrane (1 cm diameter). This was followed by light irradiation at different durations (0, 5, 10 or 20 min). Each of the membranes was then immersed for 5 min in 250 μl LB solution. Turbidity assays were carried out to evaluate bacterial growth after irradiation by adding the extracted bacterial solution to clear bottom 96-well plate, carrying out 3 repetitions for each irradiation time. OD600 values were measured using a microtiter plate reader (Varioskan Flash, Thermo) every 20 min for 18 h with a continuous shaking at 37C. Logarithmic growth curves were then plotted.

2.4. Characterization

Functional groups of the C-dots, PVDF and C-dot-PVDF composite were analyzed by ***Fourier transform infrared spectroscopy (FTIR)*** through attenuated total reflectance (ATR)-FTIR using a Thermo Scientific, Nicolet 6700 spectrometer (USA). ***Scanning electron microscopy (SEM)*** images of the composite sample were obtained on a JEOL SEM (Tokyo, Japan, JSM-7400F). For SEM imaging, the sample was coated with iridium and imaged at different magnifications. Membrane hydrophobicity was analyzed by measuring the ***water contact angles (WCA)*** using a contact angle meter (Attension Theta Lite, Biolin Scientific, Finland). The contact angles were measured with 4 μl water deposition on triplicate membrane surfaces at different positions for each sample, and average WCA was calculated. Absorbance spectra of the membranes were analyzed by ***ultraviolet–visible (uv–vis)*** absorbance measurements on a Thermo Scientific Evolution 220 spectrophotometer. Pho-

tothermal properties of the membranes were evaluated by irradiating the samples with a ***solar simulator*** (Sciencetech, AX-LA125, ASTM Class-AAA) operating at 1 kW/m^2 intensity (AM 1.5 G) in the wavelength range of 300–2000 nm. ***Thermal imaging*** of the membranes to determine the temperature before and after illumination with solar-simulated light was carried out by a thermographic camera (FLIR i7).

3. Results and discussion

Fig. 1 schematically depicts the experimental strategy for preparation of the self-sterilized C-dot-PVDF facemask membrane. C-dots, hydrothermally synthesized from citric acid and urea as the carbonaceous building blocks [28], were interspersed within a suspension of poly(vinylidene fluoride) (PVDF) at a 0.05 wt ratio (C-dot: PVDF) in dimethylformamide (DMF) and *n*-octane. Nanoporous composite free-standing C-dot-PVDF films were formed via a mixed solvent phase separation (MSPS) methodology in which the solvent mixture was heated to 85 °C, cooled at room temperature leading to solvent separation, and subsequently deposited on a solid substrate [20,21]. The resultant C-dot-PVDF matrix was stabilized through hydrogen bonding between —OH and —COOH units on the C-dots' surface and -CF_2 residues of PVDF [22,30,31]. The as-prepared C-dot-PVDF membrane could be readily attached to a commercially available cotton cloth providing effective thermal insulation. Importantly, as illustrated in Fig. 1, heat dissipated through sunlight harvesting by the embedded C-dots can lead to destruction of viral particles, without the need to external sterilization procedures.

Physico-chemical characterization of the nanoporous C-dot-PVDF film is presented in Fig. 2. The experiments outlined in Fig. 2 were specifically designed to investigate incorporation of the C-dots within the PVDF matrix and their impact upon the structural and functional properties of the polymer. (Detailed characterization of the C-dots is presented in Fig. S3). Fourier transform infrared (FTIR) spectra of the C-dots in Fig. 2A,i show the characteristic C-dots peaks corresponding to amine and hydroxyl residues in between 3200 and 3400 cm^{-1} and carbon-bonded oxygen and nitrogen between 1300 and 1600 cm^{-1} [29]. The FTIR spectrum of PVDF in Fig. 2A,ii features major signals in 1190 cm^{-1} and 1230 cm^{-1} assigned to CF_2 residues and a broad peak around 1400 cm^{-1} corresponding to CH_2 units [32]. Importantly, the FTIR spectrum of the C-dot-PVDF composite in Fig. 2A,iii reveals the distinctive peaks of the C-dots (see inset in Fig. 2A,iii; the arrows indicate the C-dot-specific signals), confirming incorporation of the C-dots within the PVDF host matrix.

Water contact angle (WCA) measurements in Fig. 2B furnish evidence for modulation of PVDF properties through C-dot incorporation. The WCA of bare PVDF membrane (not containing C-dots) was 101 ± 1° (Fig. 2B,i) accounting for the hydrophobic nature of the polymer [23,33]. In the case of the composite C-dot-PVDF, however, the WCA was reduced to 94 ± 0.4° (Fig. 2B,ii) corresponding to the presence of the more hydrophilic C-dots within the polymer matrix. Importantly, the WCA determined for C-dot-PVDF indicates that the composite membrane still retained hydrophobic surface properties, allowing for repulsion of water droplets which is essential for effective facemask materials. The scanning electron microscopy (SEM) image of the C-dot-PVDF film in Fig. 2C displays ubiquitous nanopores. The dense pore network is important for allowing efficient air flow through the membrane. Notably, the SEM analysis also reveals that pore diameters were below 100 nm (Fig. 2C, inset; size distribution determined from the SEM experimentation is presented in Fig. S4); this pore diameter threshold is crucial for effectively blocking transmission of COVID-19 viral particles (which are around 125 nm [34]). Further, the pore size distribution of the membrane and total porosity were analyzed through Brunauer-Emmet-Teller (BET) and gravimetric method respectively. The average pore diameter of C-dot-PVDF membrane obtained through BET was found to be ~49 nm (Fig. S5) and the total porosity was estimated to be 72 ± 2.4%. The stability of C-dots inside the membrane was also verified through immersing the membrane in water and spectroscopic analysis confirmed the negligible leaching of C-dots in water from C-dot-PVDF membrane (Fig. S6).

A core functionality of the new C-dot-PVDF membrane is the feasibility of self-sterilization via light absorbance and heat dissipation by the C-dots. Fig. 3 examines the photothermal properties of the membranes, in particularly the critical role of the embedded C-dots in solar-mediated heating. Fig. 3A presents the ultraviolet–visible (uv–vis) absorbance spectra of bare PVDF film and C-dot-PVDF composite membrane (C-dot: PVDF weight ratio was 0.05), respectively. The uv–vis absorbance spectra clearly show that the C-dot-PVDF membrane exhibits significantly higher absorbance in the range of 300–1000 nm. The broad absorbance range in the visible spectral region underlies the self-sterilization strategy applied here, since the light absorbed by the embedded C-dots is exploited for heat generation and concomitant destruction of viral particles.

The infrared (IR) thermal images in Fig. 3B,i and corresponding temperature variation graph in Fig. 3B,ii demonstrate the significant heat dissipation and concurrent temperature increase in the C-dot-PVDF membrane. In the experiments presented in Fig. 3B, we illuminated bare PVDF and C-dot-PVDF membranes using a solar-simulator and recorded the temperature using an infrared (IR) thermograph camera. The thermal images in Fig. 3B,i and corresponding recorded temperatures (Fig. 3B,ii) illustrate the dramatic temperature increase in the case of C-dot-PVDF membrane (from 28 °C to 66 °C after 20 min irradiation) while the temperature of the bare PVDF membrane rose from 27 °C to just 41 °C after the same irradiation time. The significant photothermal effect observed in the C-dot-PVDF membrane underscores the feasibility of self-sterilization since inactivation of Coronavirus has been reported at around 60 °C [35,36]. The on–off light irradiation experiment depicted in Fig. 3C undercores the excellent recyclability of the photothermal effects.

Fig. 4 examines the air permeability (i.e. breathability) of the C-dot-PVDF membrane and nanoparticle filtration capabilities – two core determinants for potential practical use of the composite membrane system as a facemask. The graph in Fig. 4A depicts the pressure drops measured across normal cotton fabric, surgical mask, N-95 respirator and the C-dot-PVDF membrane at air flow rates of between ~4.5 cubic feet per minute (CFM) and ~14.5 CFM, considered the recommended air flow rates for respirators [37]. The pressure drop across all film samples was found to increase in higher air flow rates [38]. Importantly, the pressure drop across the C-dot-PVDF was slightly higher than a surgical mask, and significantly lower than the standard N-95 respirator. The breathability of C-dot-PVDF membrane is ascribed to the highly porous morphology (i.e. the SEM analysis in Fig. 2C), and underscores the potential practical use of the technology in facemask applications.

Fig. 4B illustrates the capability of the C-dot-PVDF membrane to block passage of aerosolized SiO_2 nanoparticles exhibiting diameters of around 100 nm - effectively mimicking the size of viral particles (~125 nm [33]). In the experimental setup, shown in Fig. S2, we quantified the number of aerosolized nanoparticles reaching a glass slide target, with and without the C-dot-PVDF membrane placed in between the aerosol source and glass slide. The scanning electron microscopy (SEM) image in Fig. 4B,i shows ubiquitous nanoparticles on the surface of the control slide (without placement of the C-dot-PVDF membrane). However, hardly any SiO_2

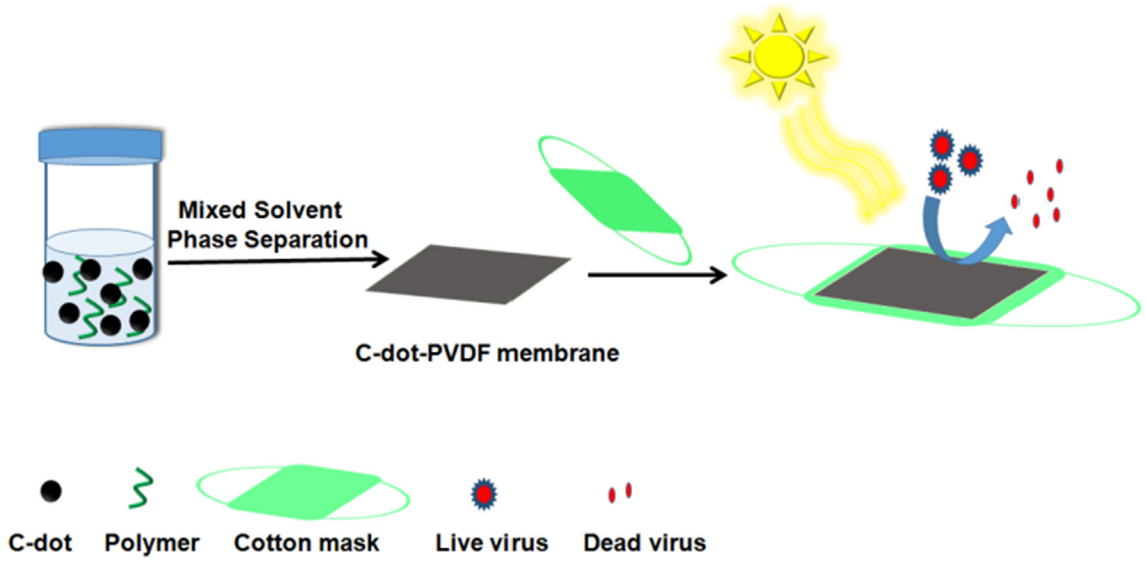

Fig. 1. Construction of the nanoporous C-dot-PVDF sunlight-mediated self-sterilizing anti-Covid-19 facemask. The C-dots and PVDF are initially dispersed in a DMF/*n*-octane mixture. A free-standing nanoporous film is formed through mixed solvent phase separation. Sunlight is absorbed by the film-embedded C-dots, resulting in heat dissipation which can be utilized for concomitant destruction of viral particles.

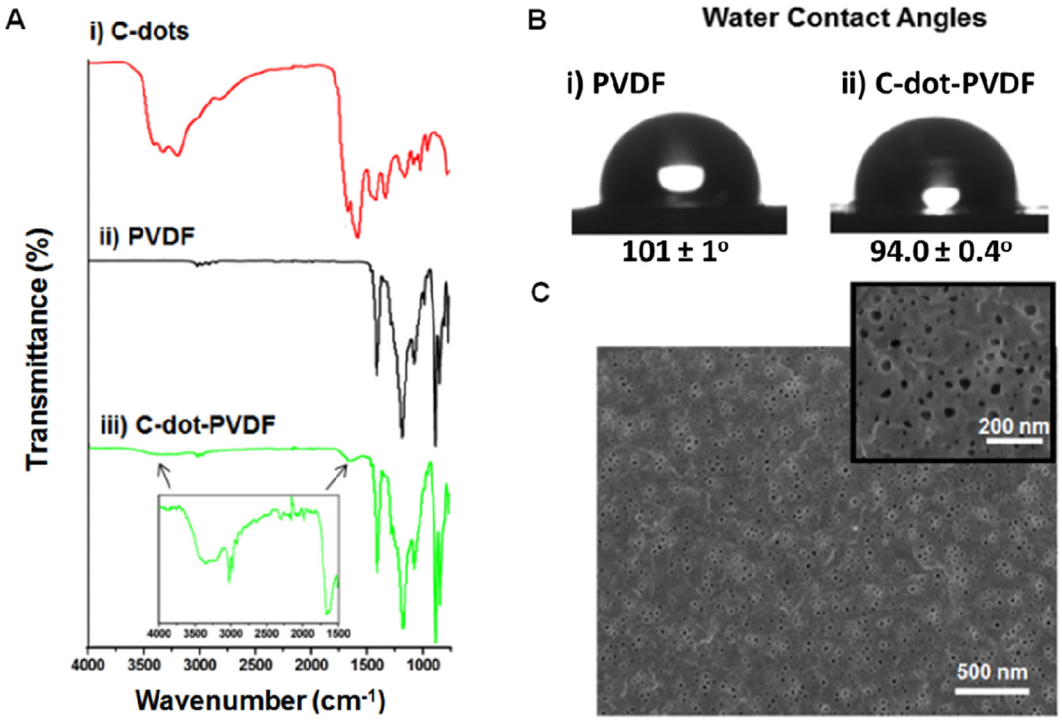

Fig. 2. Characterization of the C-dot-PVDF membrane. A. Fourier transform infrared (FTIR) spectrum of the C-dots (**i**); PVDF (**ii**), and the C-dot-PVDF composite (weight ratio 0.05 between the C-dots and PVDF) (**iii**). **B**. Water contact angle (WCA) measurements of the membrane indicating membrane hydrophobicity. **C.** Scanning electron microscopy (SEM) image of the C-dot-PVDF membrane showing abundant nanoporous morphology. Inset showing magnified SEM image.

nanoparticles were observed in the SEM image of the glass slide for which a C-dot-PVDF membrane was placed on the path of the aerosolized nanoparticles (Fig. 4B,ii). The bar diagram in Fig. 4B provides a quantitative analysis of the filtration performance, demonstrating around 97% blockage of the aerosolized nanoparticles by the C-dot-PVDF membrane, which is far better than most mask technologies.[37]

We further examined the feasibility of the solar-mediated self-sterilization strategy (Fig. 5). While viable viral particles have not been utilized (due to safety precautions), we tested *E. coli* bacterial proliferation, since these bacteria, similar to the COVID-19 virus, generally do not survive in elevated temperatures (<60C). In the experiments presented in Fig. 5, we deposited on the C-dot-PVSF membrane viable bacterial cells and irradiated the membrane for different time durations (using a solar simulator; light intensity 1 kW/m^2). Subsequent bacterial proliferation analysis (reflected in the growth curves in Fig. 5) demonstrate illumination-dependent destruction of bacterial cells adsorbed onto the C-dot-PVDF matrix, attaining complete elimination of cell viability within 20-minute illumination.

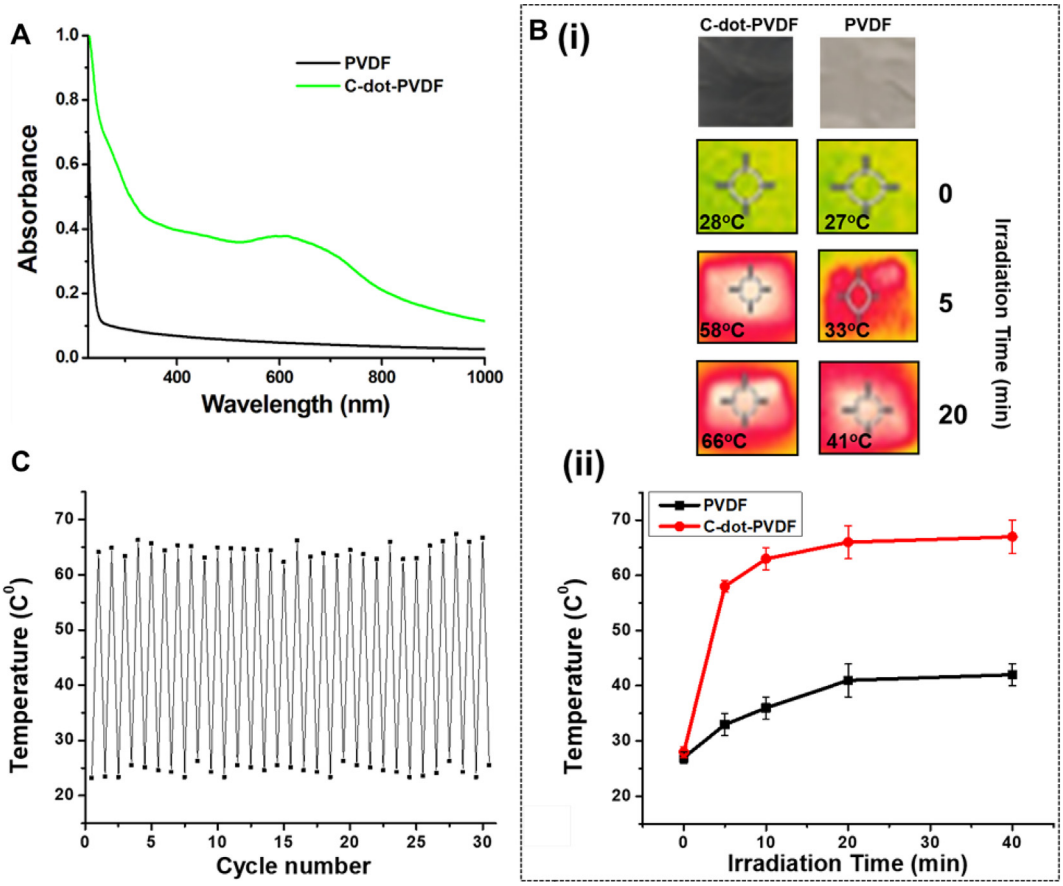

Fig. 3. Photothermal properties of the C-dot-PVDF membranes. A. uv–vis absorbance spectra of bare PVDF and C-dot-PVDF membranes. **B. (i)** Thermal images and corresponding average temperatures obtained upon irradiation of bare PVDF membrane (right) and C-dot-PVDF membrane (left) using a solar simulator (light intensity 1 kW/m^2). Significant heating occurred in the case of the C-dot-PVDF membrane. The pictures in the top row are the visual appearance of the films (Photographs of the entire films are presented in Fig. S7). **(ii)** Temperatures of the composite C-dot-PVDF and bare PVDF membranes, respectively, upon different irradiation times. Three different membranes of each sample were tested under solar irradiation. **(C)** C-dot-PVDF membrane surface temperature with on–off irradiation cycles using a solar simulator (20 min irradiation time).

4. Conclusions

This work presents the development of a new self-sterilized facemask membrane technology capable of effectively blocking and eliminating airborne biological nanoparticulates, specifically viruses such as COVID-19 and microorganisms. The nanoporous barrier comprises C-dot-PVDF membrane synthesized from readily available and inexpensive building blocks through a simple mixed solvent phase separation method. The new C-dot-PVDF films exhibit important properties required for potetial use as recyclable facemasks, including effective nanoparticle blocking, hydrophobicity, and self-sterlization. Specifically, the free-standing membrane films were hydrophobic and exhibited excellent filtration capabilities for nanoparticles in the size range of COVID-19 viral particles while attaining good breathability. Importantly, solar-induced self-sterilization could be accomplished due to the highly effective sunlight absorbance by the embedded C-dots and concomitant heat dissipation.

The C-dot-PVDF membrane technology exhibits important advantages in comparison to existing or proposed recyclable facemask systems. In particular, while published studies reported construction of films that could block viral particles [10], the adhesion of viable viruses onto the filtration surfaces poses significant health risk. Furthermore, reports on self-sterilized membrane systems [12,15] have generally described the use of chemical systems that are complex and might be harmful by themselves to the human body. Indeed, the uniqueness of the C-dot-PVDF system is due to integrating the distinct properties of the individual constituents – the nanoporosity and hydrophobicity of the polymer framework and photothermal properties of the C-dots. We envision integration of the C-dot-PVDF system with cotton cloths, furnishing commercially available recyclable anti-COVID-19 facemasks. Future expansion of the technology towards microorganism, viral, and nanoparticle filtration systems would be also feasible.

CRediT authorship contribution statement

Seema Singh: Conceptualization, Methodology, Investigation, Data curation, Visualization, Writing - original draft. **Nitzan Shauloff:** Methodology, Investigation, Validation, Visualization, Writing - original draft. **Chetan Prakash Sharma:** Investigation, Validation. **Ran Shimoni:** . **Christopher J. Arnusch:** Supervision. **Raz Jelinek:** Conceptualization, Methodology, Validation, Supervision, Writing - review & editing.

Declaration of Competing Interest

The authors declare that they have no known competing financial interests or personal relationships that could have appeared to influence the work reported in this paper.

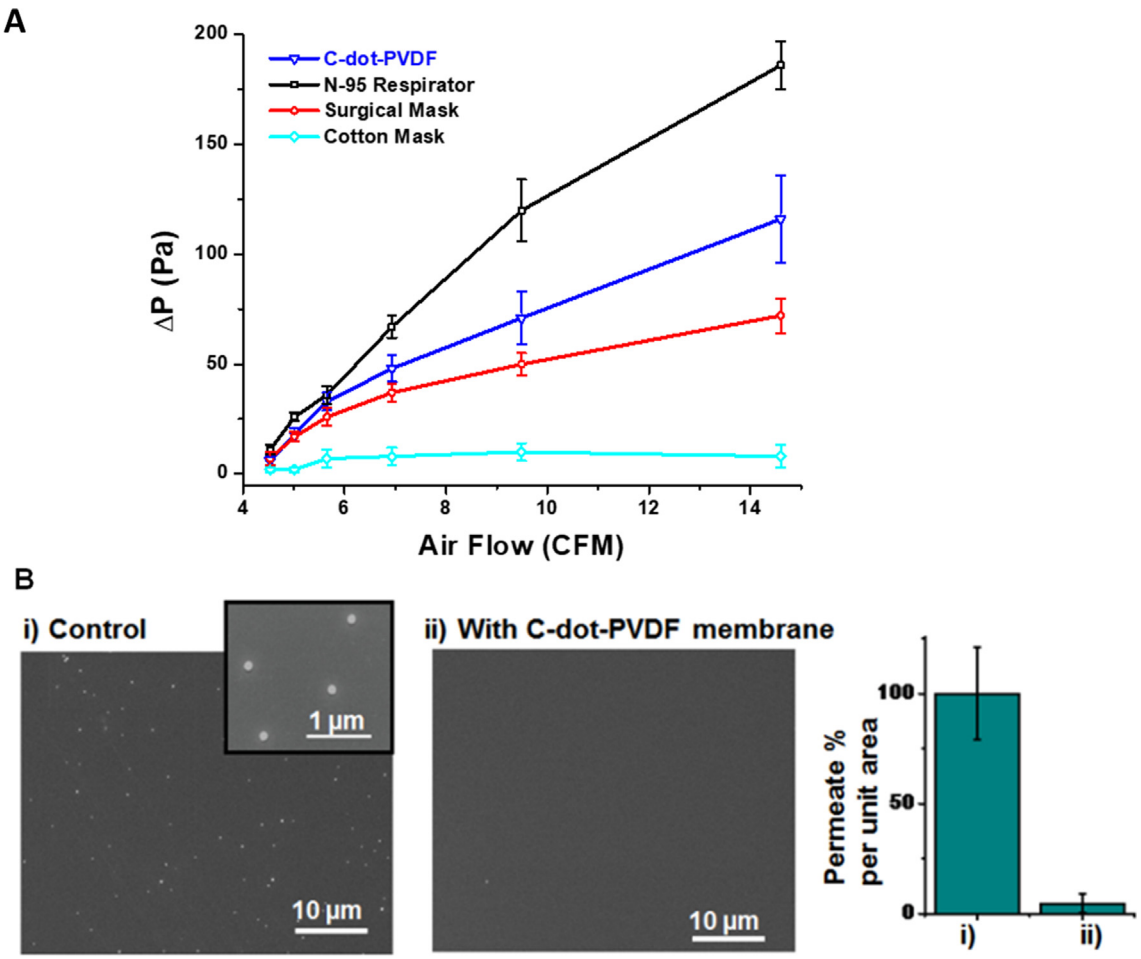

Fig. 4. Air permeability and nanoparticle filtration. A. Air permeability determined for the C-dot-PVDF membrane in comparison with commercial facemasks. Triplicates of each membrane sample were recorded **B.** Scanning electron microscopy (SEM) images of glass slides exposed to aerosolized silica nanoparticles, without the C-dot-PVDF membrane (control) and with the membrane blocking the aerosol (scheme showing the experimental setup is depicted in Fig. S2). **(i)** Control glass substrate without the membrane; the inset shows a magnified region highlighting the nanoparticles on the slide. **(ii)** Glass substrate for which the C-dot-PVDF membrane (thickness of 120 μm) was placed 10 mm above the surface. The bar diagram presents the percentage of nanoparticles per unit area on the slide, quantified from the SEM images. The results reflect calculations of 10 images from three glass slides after passing the aerosol nanoparticles with triplicate C-dot-PVDF membranes, and 10 images from the control glass slide without the membrane, defined as 100%.

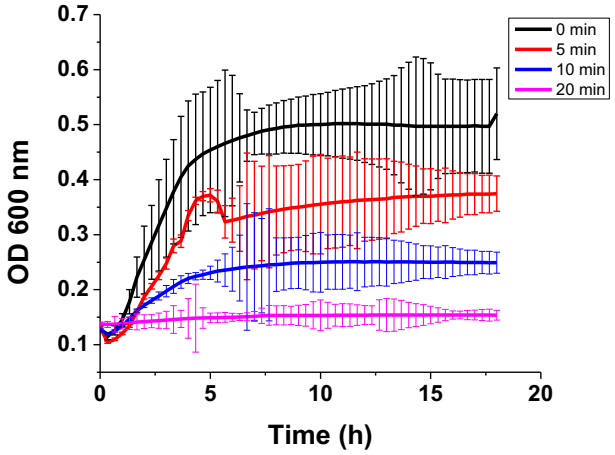

Fig. 5. Illumination-dependent bacterial viability in the C-dot-PVDF membrane. *Escherichia coli* growth curves following deposition of live bacterial cells within the C-dot-PVDF membrane and subsequent light irradiation (intensity 1 kW/m^2) for the indicated times. The bacteria were then grown in LB media.

Acknowledgement

S.S is grateful to the Marcus Fund of Ben-Gurion University for a post-doctoral fellowship

Appendix A. Supplementary material

Supplementary data to this article can be found online at https://doi.org/10.1016/j.jcis.2021.02.049.

References

[1] C.C. Lai, T.P. Shih, W.C. Ko, H.J. Tang, P.R. Hsueh, Int. J. Antimicrob. Agents 55 (2020) 105924.
[2] A.D. Workman, D.B. Welling, B.S. Carter, W.T. Curry, E.H. Holbrook, S.T. Gray, G. A. Scangas, B.S. Bleier, Int. Forum Allergy Rhinol. 10 (2020) 798–805.
[3] L. Morawska, J. Cao, Environ. Int. 139 (2020) 105730.
[4] C. Makison Booth, M. Clayton, B. Crook, J.M. Gawn, J. Hosp. Infect. 84 (2013) 22–26.
[5] N.H.L. Leung, D.K.W. Chu, E.Y.C. Shiu, K.H. Chan, J.J. McDevitt, B.J.P. Hau, H.L. Yen, Y. Li, D.K.M. Ip, J.S.M. Peiris, W.H. Seto, G.M. Leung, D.K. Milton, B.J. Cowling, Nat. Med. 26 (2020) 676–680.
[6] O.O. Fadare, E.D. Okoffo, Sci. Total Environ. 737 (2020) 140279.
[7] S. Singh, V. Prakash, Environ. Monit. Assess. 132 (2007) 67–81.
[8] WHO, Guía Interna de La OMS (2020) 1–5.
[9] W.H. Kellogg, G. MacMillan, Am. J. Public Health 10 (1920) 34–42.

[10] C.R. MacIntyre, H. Seale, T.C. Dung, N.T. Hien, P.T. Nga, A.A. Chughtai, B. Rahman, D.E. Dwyer, Q. Wang, BMJ Open 5 (2015) 1–10.
[11] S. Rengasamy, B. Eimer, R.E. Shaffer, Ann. Occup. Hyg. 54 (2010) 789–798.
[12] A. Davies, K.A. Thompson, K. Giri, G. Kafatos, J. Walker, A. Bennett, Disaster Med. Public Health Prepared. 7 (2013) 413–418.
[13] H. Zhong, Z. Zhu, J. Lin, C.F. Cheung, V.L. Lu, F. Yan, C.Y. Chan, G. Li, ACS Nano 14 (2020) 6213–6221.
[14] H. Zhong, Z. Zhu, P. You, J. Lin, C.F. Cheung, V.L. Lu, F. Yan, C.Y. Chan, G. Li, ACS Nano 14 (2020) 8846–8854.
[15] C.C. Tseng, Z.M. Pan, C.H. Chang, Aerosol Sci. Technol. 50 (2016) 199–210.
[16] D. Sachan, Chem. Eng. News 98 (31) (2020) 1469–1472.
[17] B. Gayen, S. Palchoudhury, J. Chowdhury, J. Nanomater. 2019 (2019) 19.
[18] X. Wang, Y. Feng, P. Dong, J. Huang, Front. Chem. 7 (2019) 1–9.
[19] N. Shauloff, S. Bhattacharya, R. Jelinek, Carbon 152 (2019).
[20] S. Singh, N. Shauloff, R. Jelinek, ACS Sustain. Chem. Eng. 7 (2019) 13186–13194.
[21] S. Singh, R. Jelinek, ACS Appl. Polym. Mater. 2 (2020) 2810–2818.
[22] S. Singh, R. Jelinek, Carbon 160 (2020) 196–203.
[23] G. Dong Kang, Y. Ming Cao, J. Membr. Sci. 463 (2014) 145–165.
[24] N.I.M. Nawi, H.M. Chean, N. Shamsuddin, M.R. Bilad, T. Narkkun, K. Faungnawakij, A.L. Khan, Membranes 10 (2020) 1–17.
[25] E. Ahmadi Feijani, A. Tavasoli, H. Mahdavi, Ind. Eng. Chem. Res. 54 (2015) 12124–12134.
[26] W. Cui, L. Shi, W. Song, X. Wang, Z. Lin, W. Deng, Y. Ma, J. Appl. Polym. Sci. 137 (2020) 49328.
[27] X. Yin, X. Li, X. Wang, Y. Ren, Z. Hua, Water Environ. Res. 91 (2019) 780–787.
[28] W. Zhang, Z. Shi, F. Zhang, X. Liu, J. Jin, L. Jiang, Adv. Mater. 25 (2013) 2071–2076.
[29] X. Bao, Y. Yuan, J. Chen, B. Zhang, D. Li, D. Zhou, P. Jing, G. Xu, Y. Wang, K. Holá, D. Shen, C. Wu, L. Song, C. Liu, R. Zbořil, S. Qu, Light: Sci. Appl. 7 (2018) 1–11.
[30] R.L. Thankamony, X. Li, X. Fan, G. Sheng, X. Wang, S. Sun, X. Zhang, Z. Lai, ACS Appl. Mater. Interfaces 10 (2018) 44041–44049.
[31] G. Peng, L. Xing, J. Barrio, M. Volokh, M. Shalom, Angew. Chem. – Int. Ed. 57 (2018) 1186–1192.
[32] X. Lu, Y. Peng, H. Qiu, X. Liu, L. Ge, Desalination 413 (2017) 127–135.
[33] L.N. Dumitrescu, P. Neacsu, M.G. Necula, A. Bonciu, V. Marascu, A. Cimpean, A. Moldovan, A. Rotaru, V. Dinca, M. Dinescu, Molecules 25 (2020) 582.
[34] N. El-Atab, N. Qaiser, H. Badghaish, S.F. Shaikh, M.M. Hussain, M.M. Hussain, ACS Nano 14 (2020) 7659–7665.
[35] O. Access, GMS Hyg. Infect. Control 15 (2020) 1–7.
[36] J. Han, X. Dong, Biomed. Environ. Sci. (2003).
[37] L. Janssen, N. Anderson, R. Weber, P. Cassidy, T. Nelson, J. Int. Soc. Respirat. Protect. 22 (2009). 46–46.
[38] A. Konda, A. Prakash, G.A. Moss, M. Schmoldt, G.D. Grant, S. Guha, ACS Nano 14 (2020) 6339–6347.